THE CARNEGIE INSTITUTION OF WASHINGTON is engaged in education and basic research in the physical and biological sciences. It was founded in 1902 by Andrew Carnegie and uses its resources "to encourage, in the broadest and most liberal manner, investigation, research, and discovery, and the application of knowledge to the improvement of mankind."

The Institution's program and activities are reviewed annually in May by a Board of Trustees. During the year the Board is represented by an Executive Committee, which meets quarterly. The chief administrative officer of the Institution is the President.

Administrative Offices of the Institution are at 1530 P Street, Northwest, Washington, D.C. 20005.

The Department of Terrestrial Magnetism, 5241 Broad Branch Road, Northwest, Washington, D.C. 20015, treats a wide range of studies in physics and related sciences, including astrophysics, geophysics and geochemistry, planetary physics, and nuclear and atomic physics.

The Geophysical Laboratory, 2801 Upton Street, Northwest, Washington, D.C. 20008, conducts physicochemical studies of geological problems, with particular emphasis on the processes involved in the formation and evolution of the earth's crust and mantle.

The Mount Wilson and Las Campanas Observatories are used to investigate the structure and dimensions, physical nature, chemical composition, and evolution of the universe and its components. Offices, shops, and laboratories are maintained at the headquarters at 813 Santa Barbara Street, Pasadena, California 91101. Prior to July 1, 1980, the Observatories were administered jointly with the California Institute of Technology as the Hale Observatories, which also included the Palomar Observatory and the Big Bear Solar Observatory.

The Department of Plant Biology, 290 Panama Street, Stanford, California 94305, devotes its attention to the study of photosynthesis, the means by which plants manufacture organic matter, and to the physiological and biochemical mechanisms that underlie their functional diversity and adaptations.

Research at the *Department of Embryology,* 115 West University Parkway, Baltimore, Maryland 21210, is directed toward a better understanding of the molecular and cellular mechanisms underlying differentiation, growth, and morphogenesis and the manner in which these processes are coordinated in a number of developing systems, both normal and abnormal. The Carnegie Embryological Collection is now housed in the Carnegie Laboratories of Embryology, University of California, Davis, California 95616.

Department of Terrestrial Magnetism

Washington, District of Columbia

George W. Wetherill
Director

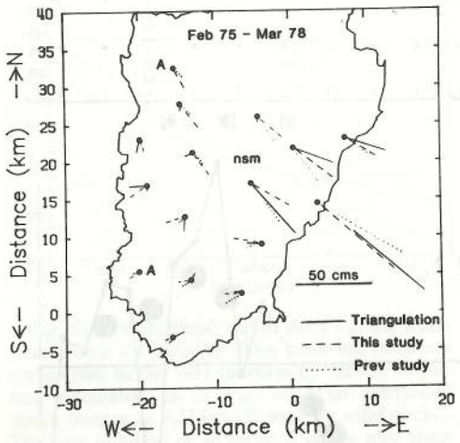

Fig. 54. Map showing stations in triangulation survey. Solid lines represent horizontal changes determined from the surveys by the Geographical Survey Institute, which assumed that stations marked A did not move. Dashed lines are horizontal displacements calculated from our model (including the F2 fault of Shimazaki and Somerville, 1978), and dotted lines show the displacements resulting from the model of Shimazaki and Somerville (1979). Station NSM is close to a nodal plane, and small changes in fault location (in particular depth of burial) will result in large changes in the calculated value for NSM displacement. Our model gives a satisfactory fit to the data, including the significant displacements near the west coast.

We find that modeling the initial activity on the Izu Peninsula as slowquakes gives good agreement with the strain data. The model is also consistent with the horizontal-displacement data and the leveling data. This study is therefore a report on the first observation of a slowquake recorded directly on more than one instrument. In addition, the interpretation is strengthened by independent measurements of crustal motions and of low acceleration features of the faulting. Thus, the existence of slowquakes has been confirmed by observations of different types of data derived from different measuring techniques. Futhermore, given adequate station coverage, we are able to determine the rupture velocity. (For F3, it is lower than for fast earthquakes by a factor of some tens.) The sequence studied here illustrates that slowquakes can be very large and therefore of importance in the redistribution of stress in seismically active regions. The F3 slowquake was in essentially the same area as the 1974 Kawazu fast earthquake. Therefore it is possible to have slowquakes or fastquakes in the same place. The incompleteness of our understanding of the mechanism of rock failure under realistic tectonic conditions is one of the major difficulties impeding a successful earthquake-prediction program.

References

Crustal Dynamics Department, Geographical Survey Institute, Crustal deformation in the central part of the Izu Peninsula (in Japanese), *Rep. Coord. Comm. Earthq. Predict.*, Geographical Survey Institute, Tokyo, *16*, 82–87, 1976.

Crustal Dynamics Department, Geographical Survey Institute, Crustal deformation in the central part of the Izu Peninsula (4) (in Japanese), *Rep. Coord. Comm. Earthq. Predict.*, Geographical Survey Institute, Tokyo, *19*, 71–75, 1978a.

Crustal Dynamics Department, Geographical Survey Institute, Crustal deformation in the Izu Peninsula (in Japanese), *Rep. Coord. Comm. Earthq. Predict.*, Geographical Survey Institute, Tokyo, *20*, 92–99, 1978b.

Inouchi, N., and H. Sato, Crustal deformation related to the Izu-Oshima Kinkai earthquake of 1978, *Bull. Geogr. Surv. Inst.*, *23*, 14–24, 1979.

Okada, Y., Fault mechanism of the Izu-Oshima-Kinkai earthquake of 1978, as inferred from the crustal movement data (in Japanese), *Bull. Earthq. Res. Inst.*, *53*, 823–840, 1978.

Sacks, I. S., S. Suyehiro, D. W. Evertson, and Y. Yamagishi, Sacks-Evertson strainmeter, its installation in Japan and some preliminary results concerning strainsteps, *Pap. Meteorol. Geophys.*, *22*, 195–208, 1971.

Sacks, I. S., S. Suyehiro, A. T. Linde, and J. A. Snoke, Stress redistribution and slow earthquakes, *Carnegie Inst. Wash. Year Book 79*, 486–491, 1980.

Sato, R., and M. Matsu'ura, Strains and tilts on the surface of a semiinfinite medium, *J. Phys. Earth*, *22*, 213–221, 1974.

Shimazaki, K., and P. Somerville, Summary of the static and dynamic parameters of the Izu-Oshima-Kinkai earthquake of January 14, 1978, *Bull. Earthq. Res. Inst.*, University of Tokyo, *53*, 613–628, 1978.

Shimazaki, K., and P. Somerville, Static and dynamic parameters of the Izu-Oshima, Japan earthquake of January 14, 1978, *Bull. Seismol. Soc. Amer.*, *69*, 1343–1378, 1979.

Tsuneishi, Y., T. Ito, and K. Kano, Surface faulting associated with the 1978 Izu-Oshima-Kinkai earthquake, *Bull. Earthq. Res. Inst.*, *53*, 649–674, 1978.

Umeda, Y., and H. Murakami, Lineament of cracking of roads due to Izu-Oshima earthquake and the area damaged by its largest aftershock (in Japanese), *Programme and Abstracts, Seismol. Soc. of Japan*, *1*, 22, 1978.

The Hekla Eruption of 1980—The Mechanism of a Ridge Volcano

R. Stefansson, I. S. Sacks, and A. T. Linde*

Iceland lies astride the mid-ocean ridge in the North Atlantic. The spreading ridge on Iceland itself is offset to the east from the submarine spreading ridges by two transform faults, one submarine to the north of Iceland, the other on land. The northern section of the on-land ridge has spread apart several meters since 1975, accompanied by volcanic activity (Krafla). The southern (submarine) extension of this ridge has also been increasingly active recently. Surtsey was formed in 1963, and Heimaey erupted in 1974.

There are two types of eruption on spreading ridges—normal volcanic eruptions and fissure eruptions. The latter consist of lava oozing out of long fissures in the ground, probably as a result of the spreading process. The eruption described here is a combination of both types.

An eruption started in the summit area of Hekla on 17 August 1980. Five minutes of steam were followed by a dark tephra column starting at 13:27 and reaching 15-km altitude. The lava flow began shortly afterwards, starting at the summit. It developed into a fissure some 7 km long, oriented northeast-southwest, trending somewhat east-west of the general trend of the spreading axis north of this region. Most of the lava issued within the first 12 hours. The preliminary estimate of the lava volume was 0.1 km^3, and the tephra (density 1–1.5 gm/cc) was 0.05 km^3. This was only a minor eruption: the period of quiescence since the previous eruption was only ten years, the shortest period since the year 1104. Contrary to expectations, very few earthquakes were recorded before the eruption. One, of magnitude 1.5, occurred about 15 minutes before, and several more were recorded in the last 10 minutes. Karl Grönvold (personal communication) supplied much useful geological information.

Seven Sacks-Evertson borehole strainmeters had been installed during the autumn of 1979 within 14–45 km of Hekla (Fig. 55), as described in *Year Book 79*, pp. 495–498. Unfortunately, stations BUR, SAU, and STO had run out of recording paper five days before the event. (This was harvest season, a very busy time for the station operators.) All stations were operating, however, within 3½–6½ hours after start of eruption. The strain records are shown in Fig. 56. We present here a preliminary study of this event; we expect to improve our modeling as further geologic and geodetic data become available.

Modeling

We have used the observations of erupted volume and fissure length to constrain our modeling. It is convenient to consider the event in three stages. During the first 24 hours, eruption and fissuring occur. In the next 24 hours, the eruption is essentially completed; the final stage (48–120 hours) is the recharge.

Stage I

This stage is characterized by the most vigorous volcanic eruptions as well as by the development of a 7-km-

*The Iceland Meteorological Office, Reykjavik.

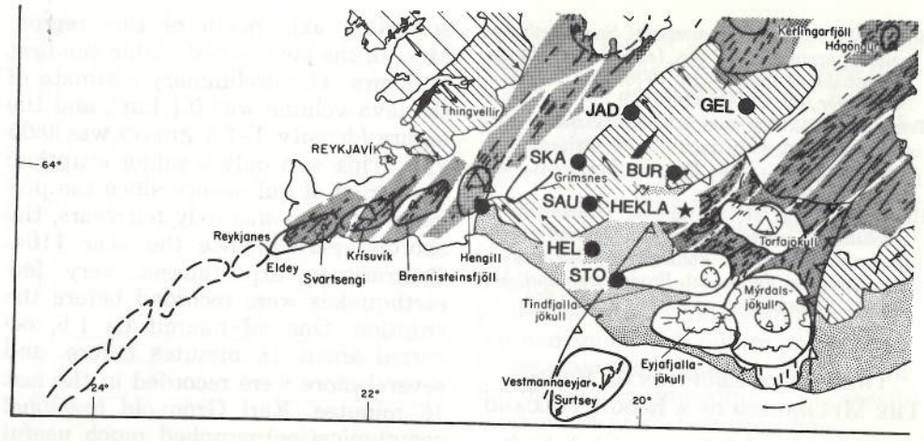

Fig. 55. Map of southwestern Iceland. The seven borehole strainmeter stations are shown with solid circles. The star marks the location of Hekla, the volcano that erupted in August 1980.

long fissure. Hekla's normal major eruption is about ten times larger than the 1980 event, and does not develop a fissure. We consider, therefore, that this eruption was triggered by a tensile (spreading) event that directly caused the fissuring. The fissure split the volcano cone.

We model this first stage as the superposition of two events: a 7-km-long tensile fracture, aligned parallel to the spreading axis, and a point-source dilatation (collapse) at depth below the volcano.

The volcanic eruption can be adequately modeled as a point-source pressure decrease at depth below the volcano. The theory was developed in *Year Book 74*, pp. 288–291. For measurements at the surface, and assuming equality of the Lamé constants λ and μ, the dilatation reduces to

$$\frac{\delta V}{2\pi[r^2+h^2]^{3/2}}\left(1-\frac{3h^2}{(r^2+h^2)}\right), \qquad (1)$$

where δV is the volume change in the magma chamber, r is the distance between the volcano and the strainmeter, and h is the depth of the magma chamber. This assumes that the incompressibility of the magma is the same as that of the surrounding rock. The volume change in the magma chamber is $(\delta P \cdot V)/K$, where δP is the excess pressure, V is the effective volume of the magma chamber, and K is the incompressibility.

Note that the strain signal (Equation 1) is proportional to the volume change, so that a large magma chamber with a small pressure change will give the same signal as a small magma chamber with a large pressure change. The volume change in the magma chamber is erupted; therefore, the strain signal is proportional to the erupted volume. We use 0.1 km^3 as the erupted volume and calculate the resultant volume strain changes at the various stations.

Added to these are the strain changes due to the fissure. We use a 7-km-long fracture and obtain the fit to the data shown in Fig. 56 by using a vertical extent of 10 km and an opening of 1 m. Figure 57 shows the volume strain field due to the fissure.

It appears that a slightly smaller erupted volume, ~0.07 km^3, would fit the data even better; the calculations may need to be redone after more detailed geological observations become available. However, the character of the data is well matched by the model.

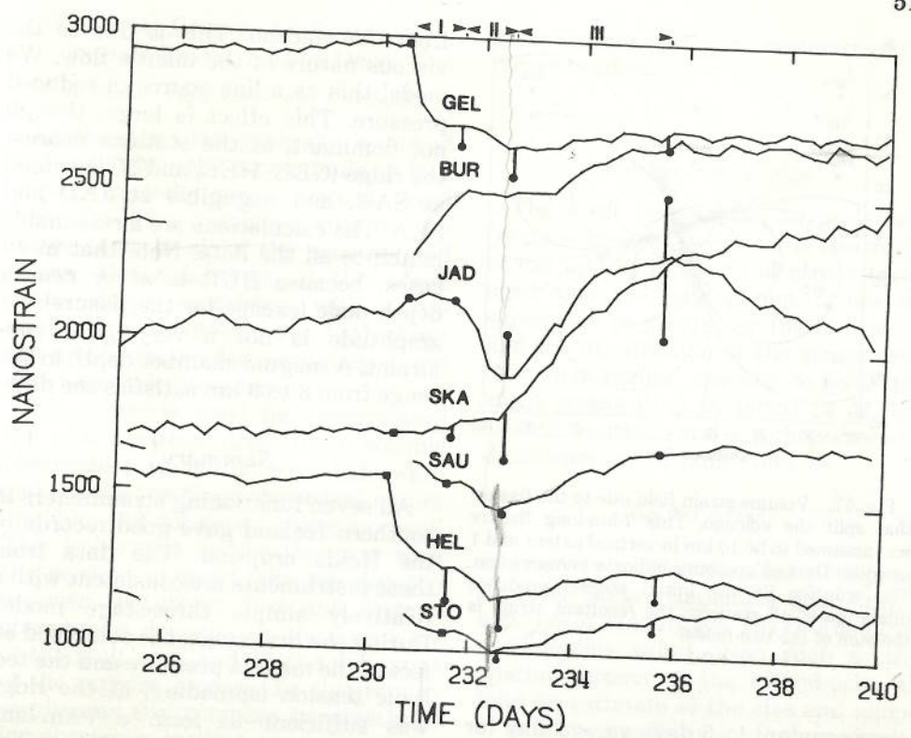

Fig. 56. Strain data from the stations shown in Fig. 55. The long-term trend of the data has been removed. The absolute value of strain has no significance; the traces are shown with arbitrary vertical spacing. The eruption began at 13:30 on day 230. We have divided the process into three sections, as indicated at the top of the figure. Values calculated from the model are shown as solid circles (the squares are arbitrary starting values). (No calculated values are given for BUR. Its sensitivity to source depth means that with slight variations in depth, we can fit the data very well.) Stage I is for an eruption of 0.1 km^3 lava as well as the opening of the 7-km-long fissure. In Stage II, we have in the magma chamber an isotropic pressure decrease one-third that of Stage I. Stage III is modeled as the recharge of the magma chamber–fissure system due to material migrating along the ridge. We assume that the magma chamber is essentially recharged.

Stage II

The second stage (day 2) has some flow (decreasing pressure) from the magma chamber but no further tearing (or spreading) of the fissure. We model it as a reduction in pressure in the vicinity of the magma chamber of about one-third that due to the first part of the eruption. Although the strain change due to this stage underestimates JAD and does not fit SKA, it fits most of the data well.

Stage III

The third stage (days 3–8) is the recharge phase. In this stage, magma flows not only to replenish the magma chamber, but also to replace the magma that filled the fissure. (Note that recharge probably starts early in the event. However, it has a longer

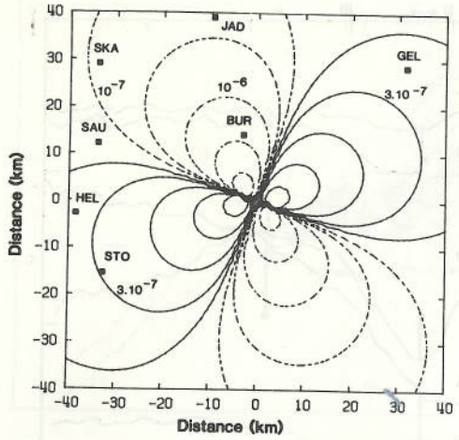

Fig. 57. Volume strain field due to the fissure that split the volcano. This 7-km-long fissure was assumed to be 10 km in vertical extent and 1 m wide. Dashed contours indicate compression. The eruption (in the initial stages) produces dilatation at all stations; the resultant strain is the sum of the two fields.

time constant [>5 days vs. <1 day for eruptive phases] so that any error from assuming that it starts after the eruption is small.) There must be a net increase in pressure in the vicinity of the volcano and fissure, but the strainmeters closest to the ridge axis, GEL in the north and HEL and STO in the south, show reduced pressure buildup during this period. We interpret this as the result of flow up (and down) the ridge axis to the eruption site. If magma rose vertically (beneath the volcano), it would cause an isotropic strain change. The small strain changes near the ridge axis suggest a viscosity-controlled recharge down the ridge. At the end of this stage, we consider that essentially all the magma displaced by the opening of the fissure and the eruption has been replaced, at least locally. We model this as a pressure recovery (point source) of a magnitude equal to that displaced in the first stage. In addition, there remains a pressure drop in the ridge "pipeline" at least at distance from the volcano. This is due to the viscous nature of the mantle flow. We model this as a line source of reduced pressure. This effect is large, though not dominant, at the stations nearest the ridge (GEL, HEL, and STO), small at SAU, and negligible at JAD and SKA. The calculations are a reasonable match to all the data. Note that in all cases, because BUR is at or near a depth node (except for the fissure), its amplitude is not a very good constraint. A magma chamber depth in the range from 6 to 9 km satisfies the data.

Summary

All seven functioning strainmeters in southern Iceland gave good records of the Hekla eruption. The data from these instruments are consistent with a relatively simple three-stage model. During the first stage, the combined effect of the magma pressure and the tectonic tension (spreading) at the ridge was sufficient to form a 7-km-long fissure, which split the volcano. The second stage was a continuation of the first, as far as a continuing reduction of pressure in the magma chamber is concerned. There was no further spreading. During the third stage, the magma chamber and the region in the general vicinity of the fissure were being recharged. The strain data indicate that most of this recharge flows up (and down) the ridge axis.

The strain data require that the associated fissure have considerable vertical depth and therefore be a significant feature of the eruption process. This suggests that regional tension is the triggering mechanism for this relatively small eruption. The immediate recovery mechanism seems to be flow along the ridge with a time constant of a few days. The data from the nearby net of strainmeters have allowed us to analyze and quantify the stages of this tectonic sequence in a manner which otherwise would not be possible.

Apparent Stress: An Estimate of the Static Stress Drop

J. A. Snoke, A. T. Linde, and I. S. Sacks*

Earthquakes are generally assumed to result when the stress buildup in a region exceeds some critical local strength. The resulting rupture releases some or all of the accumulated stress. Determinations of the static stress drops associated with earthquakes provide information both about the preconditions for earthquakes and about tectonic processes.

The methods used for determining the static stress drop from seismic observables are not as straightforward and reliable as those described earlier (pp. 493–499) for determining moment. This is because, unlike the case with the seismic moment, the relationship between the stress drop and seismic observables depends on the geometry of the fault zone and on the dynamics of the rupture process. In this report, we discuss and compare two methods for obtaining estimates of the stress drop.

The first of these methods uses static modeling to derive a relationship between the stress drop and a, a characteristic dimension of the fault zone; it then uses dynamical modeling to express a in terms of a seismic observable f_0, the "corner" frequency in the far-field displacement amplitude spectrum (see Fig. 58). The second method involves calculating a different stress parameter, called the apparent stress. Apparent stress is calculated from the ratio of radiated seismic energy to moment, both of which can be determined without recourse to specific source models. Further, it is possible to use the apparent stress as a measure of stress drop. We find that, in practice, measurement of the apparent stress gives a more consistent estimate of the stress conditions.

*Department of Geological Sciences, Virginia Polytechnic Institute and State University, Blacksburg.

Static Stress Drop Using Corner Frequency

The static stress drop, $\Delta\sigma$, is defined by $\Delta\sigma = \sigma_1 - \sigma_2$, where σ_1 is the initial stress and σ_2 is the final stress (averaged over the fault plane). If one assumes the geometry for the fault zone and the distribution of the stress drop over that region, one can express the static stress drop in terms of M, the seismic moment, and a, a characteristic dimension of the fault zone, as

$$\Delta\sigma = CM/a^3, \qquad (1)$$

where C is a dimensionless parameter of order unity (Kanamori and Anderson, 1975; Madariaga, 1977). For large earthquakes, information such as the spatial pattern of the aftershocks allows an estimate of the size and shape of fault region; Equation 1 thus gives a fairly reliable estimate of the static stress drop averaged over the fault zone (Kanamori and Anderson, 1975). Note that this assumes the aftershock zone to be a direct measure of the fault area; there are cases in which the aftershock zone increases with time.

More often, however, the only data available are seismograms of the event to be studied. When this is the case, one must assume a fault geometry and attempt to estimate a from the seismograms. Historically, many geometries ranging from long, narrow rectangles to circles have been assumed. However, provided the aspect ratio is not extreme, C will not vary by more than a factor of two for different geometries. We will assume, along with many other researchers (e.g., Brune, 1970; Madariaga, 1976; Boatwright, 1980), a circular geometry. For a uniform stress drop on a circular region of radius a, $C = 1.374$ (Eshelby, 1957; Keilis Borok, 1959).

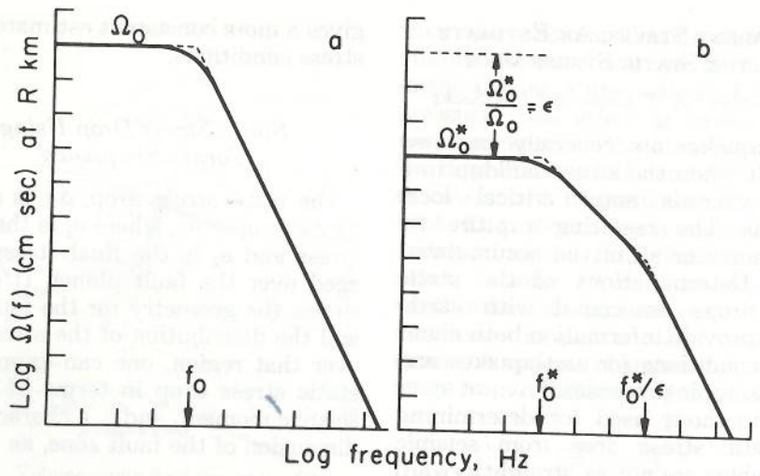

Fig. 58. The far-field shear displacement spectra of Brune (1970) for two seismic sources having the same source dimension and effective stress (the difference between the initial stress and the frictional stress opposing motion). (a) $\epsilon = 1$ (100% efficiency); the final stress is the same as the frictional stress. (b) $\epsilon < 1$; the final stress is greater than the frictional stress. These curves are typical of the spectral shapes predicted by most source models. (After Hanks and Thatcher, 1972.)

The most common method to estimate a is to assume a dynamical rupture model which gives a relationship between a and the shape of the far-field displacement amplitude spectrum. Most such spectra can be fit reasonably well by one of the model spectra shown in Fig. 58. The relationship can be expressed in the following form:

$$a = y/f_0, \tag{2}$$

where f_0 is the "corner" frequency and y is a parameter which, in general, increases monotonically with the signal and rupture velocities.

The advantage of this procedure is that many spectra can be fit by the model spectra; the method is thus easy to apply. The disadvantages are that (1) models with considerably different parameterizations for C and k may lead to the same spectra (this includes multiple events erroneously interpreted as single events [Linde *et al.*, 1975]), and (2) since the stress drop depends on a^3 (Equation 1), it follows that uncertainties in determining a can result in large variations in estimates for the stress drop. An example which illustrates this point is the large spread in stress drop found by Tucker and Brune (1973) in their plot of moment vs. source dimension for a high-quality data set of aftershocks of the San Fernando earthquake.

The Apparent Stress

The apparent stress (e.g., Savage and Wood, 1971) is given by

$$\sigma_{app} = \epsilon\bar{\sigma} \tag{3a}$$

$$= \mu E/M, \tag{3b}$$

where $\bar{\sigma} = (\sigma_1 + \sigma_2)/2$ represents the average stress, ϵ the seismic efficiency (radiated energy divided by total elastic energy involved in the faulting process), E the radiated energy, and μ the rigidity.

For digital (or analog-tape) recordings from a broad-band seismograph, the radiated energy determination should be as stable as the moment determination. The radiated energy is proportional to the integral of the square of the far-field velocity spectrum. Given an adequate signal-to-noise ratio for about a decade on either side of the corner frequency, the determination of this integral is in fact more objective than the estimate of the low-frequency level used in the moment determination. (Boatwright [1980] points out that directivity and diffraction effects may lead to erroneous results if not taken into account when calculating the energy, but these effects seem to apply only to a small part of the focal sphere and are not usually considered.)

Until recently, most seismograph systems were not of sufficient quality to allow reliable radiated energy determinations, so an alternative method for estimating the radiated energy has been employed: a magnitude-energy relation such as that proposed by Gutenberg and Richter (1942). However, the approximate nature of such relationships and their lack of universality prompted researchers, such as Thatcher and Hanks (1973), to give apparent stress reduced weight.

Recent studies (Stefansson *et al.*, 1979; Boatwright, 1981a,b) have used apparent-stress determinations based on data from seismographs with adequate passbands to make reliable energy determinations. In particular, the Stefansson *et al.* study of suites of smaller earthquakes preceding a major Icelandic earthquake found the apparent stress to be quite stable (varying by less than a factor of three for each suite) and having temporal and spatial trends of possible tectonic significance.

The Relationship between Apparent Stress and the Static Stress Drop

Savage and Wood (1971) show that if one assumes that σ_2, the final stress, is less than or equal to σ_f, the frictional stress opposing motion on the fault, then, defining

$$\eta = \sigma_{app}/\Delta\sigma,$$

they show that

$$\eta \leq 0.5. \tag{4}$$

Although not all models make this assumption (e.g., Brune's model for $\epsilon < 1$ as in Fig. 58b), the results from observations seem consistent with this inequality (e.g., Savage and Wood, 1971; Aki, 1972). In the simpler and most often applied form of Brune's model (Fig. 58a), the final stress is the same as the frictional stress. In this case, the inequality in Equation 4 becomes an equality, so that an estimate of the apparent stress is equivalent to an estimate of the static stress drop.

Sato and Hirasawa (1973) developed a model which is essentially a kinematic version of Brune's model but with a subsonic rupture velocity. (Brune assumed an instantaneous rupture.) In the context of this model, they derive a dependence of η on the rupture velocity (Fig. 59).

Because of the difficulties raised by model-dependent assumptions in previous studies, we have chosen a different approach—one basically empirical and as free of assumptions as possible. It is now clear that the spectral character of an earthquake's radiated energy can, in general, be represented by a shape similar to that shown in Fig. 58a. Such a displacement amplitude spectrum can be divided into three parts: a low-frequency constant amplitude section, an intermediate-frequency section in which the amplitude is proportional to a negative power (usually -1) of frequency, and a high-frequency region in which the amplitude decreases more rapidly (f^{-2} or faster). By parameterizing this spectrum in terms of the characteristic (corner) frequency at which the low and intermediate regions meet, we derive

$$\sigma_{app} = Mgf_0^3, \quad (5)$$

where g depends only on the (observed) shape of the spectrum. This relation is independent of any model assumptions. We can determine the stress ratio η by combining Equations 1, 2, and 5:

$$\eta = gy^3/C, \quad (6)$$

where C is approximately constant and y is a function of the rupture and signal velocities.

Concluding Remarks

Studies of stress drop have typically yielded wide variability for the stress values; it now appears that apparent stress can be determined with greater reliability. Apparent stress can be calculated without recourse to specific models and is related to stress drop through a model-dependent relation (Equation 6). However, the model-dependent factor y in this relation is the same factor that appears in the stress drop calculation. Because of this, and because of the stability of the apparent-stress determinations of Stefansson *et al.*, we suggest that, provided the quality of the available data is sufficient, the apparent stress is the preferred parameter for stress determination.

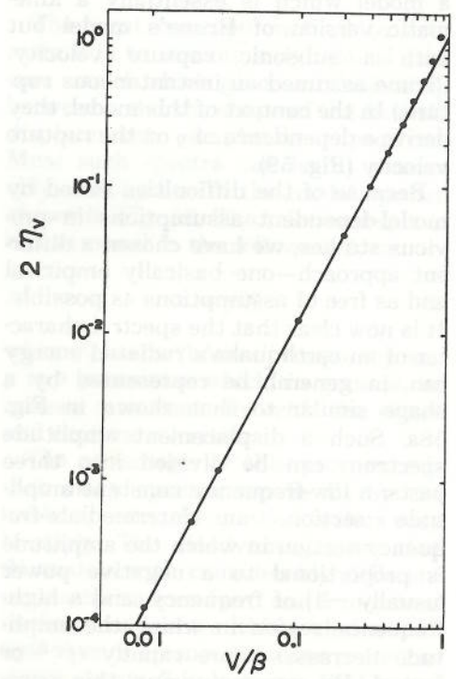

Fig. 59. A plot of 2η, the parameter defined by Equation 6 as a function of the rupture velocity divided by the shear-wave velocity. (After Sato and Hirasawa, 1973.)

References

Aki, K., Earthquake mechanism, *Tectonophysics, 13,* 423–446, 1972.

Boatwright, J., A spectral theory for seismic sources: simple estimates of source dimension, dynamic stress drop and radiated seismic energy, *Bull. Seismol. Soc. Amer., 70,* 1–26, 1980.

Boatwright, J., Quasidynamic models of simple earthquakes: application to an aftershock of the 1975 Oroville, California earthquake, *Bull. Seismol. Soc. Amer., 71,* 69–94, 1981a.

Boatwright, J., The effect of rupture complexity on estimates of stress release, *Trans. Amer. Geophys. Union, 62,* 592, 1981b.

Brune, J. N., Tectonic stress and the spectra of seismic shear waves from earthquakes, *J. Geophys. Res., 75,* 4997–5009, 1970; Correction, *J. Geophys. Res., 76,* 5002, 1971.

Eshelby, J. D., The determination of the elastic field of an ellipsoidal inclusion and related problems, *Proc. Trans. Roy. Soc. London, Ser. A, 241,* 376–396, 1957.

Gutenberg, B., and C. F. Richter, Earthquake magnitude, intensity, energy and acceleration, 2, *Bull. Seismol. Soc. Amer., 32,* 163–191, 1942.

Hanks, T. C., and W. Thatcher, A graphical representation of seismic source parameters, *J. Geophys. Res., 77,* 4393–4405, 1972.

Kanamori, H., and D. L. Anderson, Theoretical basis of some empirical relations in seismology, *Bull. Seismol. Soc. Amer., 65,* 1073–1095, 1975.

Keilis Borok, V., On estimation of the displacement in an earthquake source and of source dimensions, *Amer. Geofis. (Rome), 12,* 205–214, 1959.

Linde, A. T., I. S. Sacks, and J. A. Snoke, Multiple rupture earthquakes and the determination of source parameters, *Carnegie Inst. Wash. Year Book 74,* 281–286, 1975.

Madariaga, R., Dynamics of an expanding circular fault, *Bull. Seismol. Soc. Amer., 66,* 639–666, 1976.

Madariaga, R., Implications of stress-drop models of earthquakes for the inversion of stress drop from seismic observations, *Pure Appl. Geophys., 115,* 301–316, 1977.

Sato, T., and T. Hirasawa, Body wave spectra from propagating shear cracks, *J. Phys. Earth, 21,* 415–431, 1973.

Savage, J. C., and M. D. Wood, The relation between apparent stress and stress drop, *Bull. Seismol. Soc. Amer., 61,* 1381–1388, 1971.

Stefansson, R., I. S. Sacks, and A. T. Linde, Stress field changes during a tectonic episode in northern Iceland, *Carnegie Inst. Wash. Year Book 78,* 320–325, 1979.

Thatcher, W., and T. C. Hanks, Source parameters of southern California earthquakes, *J. Geophys. Res., 78,* 8547–8576, 1973.

Tucker, B. E., and J. N. Brune, Seismograms, S-wave spectra, and source parameters for aftershocks of San Fernando, California, earthquake of February 9, 1971, in *Geological and Geophysical Studies, III,* (U.S. Department of Commerce), 69–121, 1973.

METEORITES AND METEOROIDS

. . . the might
Of earth-convulsing behemoth, which once
Were monarch beasts, and on the slimy shores
And weed-overgrown continents of earth,
Increased and multiplied like summer worms
On an abandoned corpse, till the blue globe
Wrapped deluge round it like a cloak, and they
Yelled, gasped and were abolished; or some God
Whose throne was in a Comet, passed and cried—
"Be not!" and like my words they were no more.

Shelley (1820)

Impacts of Extraterrestrial Bodies on the Earth and Moon

*G. W. Wetherill and D. O. ReVelle**

The discovery of geochemical evidence in support of the hypothesis that major biological extinctions, including that of the dinosaurs, were triggered by the impact of asteroidal or cometary objects has led to widespread interest in the flux of extraterrestrial bodies upon the Earth (Alvarez *et al.*, 1980). Whether or not this particular hypothesis turns out to be correct, it is now more generally recognized that an understanding of the nature of these impacting objects, the geological and meteorological effects of their impact, the dynamical processes that brought them to the Earth, and of their source in the solar system, is central to many problems in earth and planetary science.

Every year about a thousand tons of extraterrestrial matter collide with the Earth. On the longer scale of geological time, a body 10^{12} tons in mass strikes the Earth about once per 100 million years, releasing an energy equivalent to a million 50-megaton nuclear weapons. During the earliest phase of Earth history, the Earth itself probably accumulated by impacts of this kind. Later manifestations of these events are the cratered surfaces of the Moon and terrestrial planets, great atmospheric explosions like that in Tunguska, Siberia, in 1908, and the meteorites in our museums and laboratories.

*Physics Department, Northern Arizona University, Flagstaff.